FRA-75-2

REPORT NO. FRA-OR&D-75-72

A STUDY OF LINEAR INDUCTION MOTOR CHARACTERISTICS: THE OBERRETL MODEL

John J. Stickler

MAY 1975

INTERIM REPORT

Prepared for

U.S. DEPARTMENT OF TRANSPORTATION

FEDERAL RAILROAD ADMINISTRATION

Office of Research and Development

Washington DC 20590

Technical Report Documentation Page

1. Report No.	2. Government Accession No.	3. Recipient's Catalog No.
FRA-OR&D-75-72		

4. Title and Subtitle	5. Report Date
A STUDY OF LINEAR INDUCTION MOTOR CHARACTERISTICS: THE OBERRETL MODEL	May 1975
	6. Performing Organization Code
7. Author(s) John J. Stickler	8. Performing Organization Report No. DOT-TSC-FRA-75-2
9. Performing Organization Name and Address U.S. Department of Transportation Transportation Systems Center Kendall Square Cambridge MA 02142	10. Work Unit No. (TRAIS) RR505/R5316
	11. Contract or Grant No.
12. Sponsoring Agency Name and Address U.S. Department of Transportation Federal Railroad Administration Office of Research and Development Washington DC 20590	13. Type of Report and Period Covered Interim Report Sept. 1973-March 1974
	14. Sponsoring Agency Code

15. Supplementary Notes

16. Abstract

The Oberretl theory of the double-sided linear induction motor is examined, starting with the idealized model and accompanying assumptions, and ending with relations for predicted thrust, airgap power, and motor efficiency. The effect of varying the maximum transverse harmonic order on the transverse primary current density and airgap flux density is considered. The Oberretl theory is seen to lead to excessively large flux densities in the regions adjacent to the primary which results in an overestimate of the normal attractive forces at small motor slip frequencies.

A comparison of the LIM forces predicted by the Oberretl and Elliott models is given for the TLRV and LIMRV LIMs. The Oberretl theory gives thrust in good agreement with those of Elliott for the LIMRV; for the TLRV, the Oberretl theory predicts thrust about 20 percent greater than those predicted by Elliott. The corresponding normal forces predicted by the Oberretl theory were approximately three times greater than those predicted by Elliott.

A computer program developed as part of this study program is given in the appendix. It requires computing times of the order of 50 seconds for typical runs consisting of ten case points.

17. Key Words
Linear Induction Motor
LIM Propulsion Characteristics
End-Effect

19. Security Classif. (of this report)	20. Security Classif. (of this page)	21. No. of Pages	22. Price
Unclassified	Unclassified	48	

PREFACE

This report discusses the Oberretl three-dimensional model of linear induction motors and its application to the analysis of the high-speed propulsion characteristics of linear induction motors. It comprises the first in a three part series devoted to a review of current LIM theories and the presentation of computer programs based on these theories. The remaining reports of this study will treat the theoretical approaches adapted by S. Yamamura and H. Mosebach in their linear induction motor analyses. Each report has as its primary objective the comparison of the relative propulsion characteristics predicted by each theory and an examination of their differences as they relate to the models used in each theory.

The author is pleased to acknowledge the following individuals for numerous discussions and helpful information: Mr. Matthew Guarino, Jr. of the U.S. Federal Railroad Administration, Dr. Clem Skalski of MITRE Corporation, Dr. David G. Elliott of the Jet Propulsion Laboratory, and Professor James Melcher of the Massachusetts Institute of Technology.

SYMBOL	
b	Secondary thickness
B	Flux density
c	Half-width of primary (stator)
F_x	Thrust (along x direction)
$F(\nu,n)$	Thrust harmonic
g	Airgap separating primary and secondary
h	Distance beyond primary edge defining effective decay distance of primary mmf.
I_1	Stator coil current per phase
J	Primary current density
k	Index defining phase number
k_x, k_z	Fundamental wavenumber components in x, z directions
$^{\nu}k_w$	νth harmonic of (longitudinal) winding factor
l	Length of periodic cell in longitudinal (x) direction
L	Width of periodic cell in transverse (z) direction
l_1	Longitudinal mmf gap length
l_s	Motor length
m	Number of primary phases
n	Transverse harmonic order
N	Turns per coil
P	Number of LIM poles
q	Number of coils in coil group (phase belt)
s	Slip
$^{\nu}s$	Effective slip of νth mmf harmonic wave
V	Motor speed
x	Longitudinal (thrust) direction

Y	Normal direction to primary surface
z	Transverse direction
α	Slot pitch in radians
α_z	Primary sheet current density in z direction
ε	Parameter defining stator pole pitch
κ	Index defining coil in given coil group
λ	Wave number in airgap in direction normal to primary
μ_o	Permeability of free space
μ_2	Permeability of secondary
ν	Longitudinal harmonic order
ρ	Index defining coil group in given phase
σ_2	Secondary conductivity
ω	Angular frequency

TABLE OF CONTENTS

LIST OF ILLUSTRATIONS

1. INTRODUCTION

Recent interest in linear induction motor applications for high-speed ground transportation has stimulated a number of theoretical investigations of single- and double-sided linear induction motors (LIMs). As a result of these investigations, different mathematical LIM models have been developed which are useful in estimating the performance characteristics of actual LIMs. Computers are required, in most cases, to effectively implement these studies, due to the magnitude of the calculations involved in such studies. One principal objective of the FRA electrical propulsion program is the investigation of various LIM models using computer programs specifically developed for this purpose and based on theories representative of each model.

The most promising mathematical models presently available for consideration are those developed by K. Oberretl (Brown-Boveri Co, Zurich, Switzerland), S. Yamamura (University of Tokyo, Tokyo, Japan), and H. Mosebach (University of Braunschwieg, Braunschweig, West Germany). All these models describe a LIM with finite primary current excitation, i.e., a primary with finite length and width. The Mosebach model has the additional refinement of a finite ferromagnetic primary region. A comparison of the LIM reaction forces predicted by each of the above models will provide information on boundary related effects (edge-effects, end-effects) and their influence on LIM performance as predicted by each model.

Each of the above mathematical models will be examined and discussed separately in individual reports. The first model to be examined is the Oberretl model[1] as it relates to a double-sided LIM with constant current excitation. This report, which is devoted to a study of the Oberretl theory, discusses different aspects of the theory in separate sections. Section 2.1.1 examines the criteria for choosing the mmf gap in the LIM periodic cell, Section 2.1.2 the expression for the stator

winding factor as derived by Oberretl, Section 2.1.3 the amplitude spectrum of the primary current, Section 2.1.4 the amplitude spectrum of the thrust harmonics, and Section 2.1.5 the predicted airgap flux density along the transverse axis of the LIM. In the second part of the report, a summary is given of the computed reaction forces (thrust, normal forces) for the tracked levitated research vehicle (TLRV) and the linear induction motor research vehicle (LIMRV) motors. Whenever possible, a comparison is presented between the forces predicted by the Oberretl model and those predicted by D. Elliott.[2] The final part of the report summarizes the significant results of the study and the problems involved in the application of the Oberretl theory to high-speed LIMs.

2. TECHNICAL DISCUSSION

2.1 THE OBERRETL MODEL

The Oberretl treatment of linear induction motors begins by replacing the actual LIM with a three-dimensional model, combining a two-dimensional Fourier mmf-distribution with an exact solution of the diffusion equation along the direction normal to the primary surface. The mmf is developed by superimposing mmf contributions from an infinite array of adjacent primary elements lying in the plane of the stator. This leads to a Fourier series representation for the total mmf equal to the sum of an infinite number of (mmf) harmonics, each defined by its respective harmonic-order along the longitudinal and transverse wave vector directions. To limit the time required for numerical computations, a limit is imposed on the maximum number characterizing the series. The choice of the values of maximum harmonic number represents a compromise between excessive computing time and sufficient harmonics required to describe adequately the mmf-distribution. The airgap flux density, which is also expressed in a Fourier Series, is derived from the magnetic vector potential with suitable prescribed boundary conditions. LIM thrust and normal forces are determined by integrating the Maxwell Stress Tensor over the region bounded on one side by the secondary.

The Oberretl model is based on the following assumptions:

a. Current densities normal to the primary and secondary members are zero. Current flow in the primary and secondary elements lies in a plane parallel to the primary.

b. The permeability of the primary is infinite.

c. Edge-effects associated with the primary ferromagnetic region are neglected; i.e., magnetic end-effects are absent. Only end-effects associated with finite "winding current" distributions are included in the analysis.

d. The active primary current density is constant along the transverse direction within the confines of the primary (stator) and decays to zero at a distance, h, beyond the primary edge according to $1 - \sin \frac{(z-c)\pi}{2h}$, where z is the transverse distance relative to the primary midplane and c is the half-width of the primary element. As pointed out by Oberretl, other current density functions could be substituted for the above, provided they relate correctly to measured field distributions.

e. The mmf and flux density distributions are periodic functions of distance along the longitudinal and transverse directions of the motor. To develop this periodicity, mmf gaps are inserted at periodic positions along the longitudinal and transverse axes of the motor.

2.1.1 Criteria for Choosing Longitudinal mmf Gap

The Oberretl theory inserts an mmf gap adjacent to the primary in order to develop an mmf-distribution function which is periodic along the longitudinal (and transverse) axis of the motor. The choice of longitudinal gap length is critical in that too small a gap length causes unrealistic oscillations in the thrust-frequency characteristic while too large a gap length results in an unreasonably long computation time. The criteria adopted in choosing the gap length is that the length be sufficiently long to allow the end-effect wave to decay to a small value. A choice of gap length equal to twice the decay length of the end-effect wave appears to be a reasonable compromise.

The decay length of the principal end-effect wave is given approximately by the reciprocal of the following quantity,[3]

$$\text{REAL}\left(\frac{\mu_o V}{2\rho_s g} - \frac{1}{2}\sqrt{\left(\frac{\mu_o V}{\rho_s g}\right)^2 + j\,\frac{4\omega\mu_o}{\rho_s g}}\right) \qquad (1)$$

for LIMs having a pole gap separation g, secondary surface resistivity ρ_s, stator excitation frequency ω, and motor speed V relative to the secondary rail. For the TLRV LIM operating at 300 mph and a frequency of 165 Hz, the computed decay length was

11 meters; for the LIMRV operating at 250 mph and a frequency of 165 Hz, the computed decay length was 7.3 meters. See page 2 for a summary of motor parameters describing the respective motors. In the computer studies of the TLRV and LIMRV motors, the respective gap lengths chosen were 33.212 and 11.096 meters.

2.1.2 Primary Winding Factor

Oberretl expresses the primary mmf, $\theta(x,t)$, in terms of the sum of mmfs of each coil described by

$$\theta(x,t) = j \frac{2NI_1\sqrt{2}}{\pi\nu} {}^{\nu}k_w \, e^{\,j\left(\omega t - \nu x + \nu\beta + \pi/m\right)} \tag{2}$$

${}^{\nu}k_w$ is the winding factor associated with the νth harmonic, β is the phase angle of the harmonic, m is the number of phases in the winding, and N is the number of turns in each coil. The derivation of ${}^{\nu}k_w$ follows from summing the mmf contributions of each coil described by

$$\nu_\theta = \frac{NI\sqrt{2}}{\pi\nu}\sin\nu(mq-\varepsilon)\frac{\alpha}{2}\, e^{j\left[\omega t - \nu x - (k-1)\frac{2\pi}{m} + \nu(K-1)\alpha\right.}$$

$$\left. + \nu(\rho-1)mq\alpha + \nu(k-1)2q\alpha\right] \tag{3}$$

Here α is the slot pitch in radians, k denotes the phase number, q denotes the particular coil in a given phase group, and ε is the reduction in width of the coils (coil pitch) in units of slots. For a double-layer winding with half-filled end slots, there exist

1, 2,.....k....m phases

1, 2,.....K....q coils in each coil group

1, 2,.....ρ....p* coil groups per phase

*Note that Oberretl uses p to denote pole pairs.

The values of k, K, and ρ are illustrated below for the "forward-connected" coils for a stator winding having two coils/phase, three phases, two poles (one pole pair), and a two-thirds pole pitch. The corresponding parameters for the "reverse-connected" coils are not shown, but are easily obtained from Equation 3 and the definition of the parameters.

ρ =	1		1		1		3		3		3										
K =	1		2		3		1		2		3										
K =	1	2	1	2	1	2	1	2	1	2	1	2	1	2	1	2	1	2	1	2	1	2
	A	A	$\bar{C}$	$\bar{C}$	B	B	$\bar{A}$	$\bar{A}$	C	C	$\bar{B}$	$\bar{B}$	A	A	$\bar{C}$	$\bar{C}$	B	B	$\bar{A}$	$\bar{A}$	C	C	$\bar{B}$	$\bar{B}$
			$\bar{A}$	$\bar{A}$	C	C	$\bar{B}$	$\bar{B}$	A	A	$\bar{C}$	$\bar{C}$	B	B	$\bar{A}$	$\bar{A}$	C	C	$\bar{B}$	$\bar{B}$	A	A	C	C	B	B

The series summation of coils in a phase group leads to

$$\frac{\sin q\frac{\nu\alpha}{2}}{\sin\frac{\nu\alpha}{2}} e^{j(q-1)\frac{\nu q\alpha}{2}}$$

The series summation of phase groups associated with the m phases of the primary yields

$$\frac{\sin m(\nu q\alpha-\pi/m)}{\sin (\nu q\alpha-\pi/m)} e^{j(m-1)(\nu q\alpha-\pi/m)}$$

The series summation of the coil groups of a given phase gives

$$\frac{\sin \frac{P}{2} \nu m q\alpha}{\sin \nu m q\alpha} e^{j\left(\frac{P}{2}-1\right)m\nu q\alpha}$$

Finally, the "reverse-connected" coil groups are related to the "forward-connected" coil groups by the factor

$$1 - \exp^{j(\nu mq\alpha-\pi)} = 2j \sin\frac{\nu mq\alpha}{2}$$

since the "reverse-connected" coil groups are both spatially and electrically 180 degrees out-of-phase relative to the "forward-connected" coil groups. Combining the above factors into a single expression, Oberretl obtains (Ref. 1, p. 7)

$$k_{w_\nu} = \frac{\sin\frac{P}{2}\nu mq\alpha}{\sin\nu mq\alpha}\ \sin\frac{\nu mq\alpha}{2}\cdot\frac{\sin q\nu\alpha/2}{\sin\nu\alpha/2}\cdot\sin\frac{\nu mq-\varepsilon}{2}\cdot\frac{\sin m(\nu q\alpha-\pi/m)}{\sin(\nu q\alpha-\pi/m)} \quad (4)$$

The above equation is not valid for a LIM with odd numbers of poles since it gives infinitely large k_{w_ν} values when $\nu mq\alpha \to \pi$.

An alternate expression for the winding factor which is valid for both even and odd numbers of motor poles can be derived by summing the mmf contributions first within a pole pitch and next over the number of half-wavelength contributions comprising the motor. Thus summing the coil groups within a pole pitch gives

$$\sum_{k=1}^{m} e^{j\left[-(k-1)\frac{\pi}{m}+\nu(k-1)q\alpha\right]} = \frac{\sin\frac{m}{2}(\nu q\alpha-\pi/m)}{\sin\left(\frac{\nu q\alpha-\pi/m}{2}\right)}\cdot e^{j\frac{(m-1)}{2}\left(\nu q\alpha-\frac{\pi}{m}\right)}$$

and summing the respective pole-pitch contributions over the entire length of the motor yields

$$\sum_{\rho=1}^{P} e^{j\left[\nu(\rho-1)mq\alpha+(\rho-1)\pi\right]} = \frac{\sin P\frac{\nu mq\alpha-\pi}{2}}{\sin\frac{\nu mq\alpha-\pi}{2}}\cdot e^{j(P-1)\left(\frac{\nu mq\alpha-\pi}{2}\right)}$$

This leads to the following expression for the winding factor

$$k_{w_\nu} = \frac{\sin P\frac{\nu mq\alpha-\pi}{2}}{\sin\frac{\nu mq\alpha-\pi}{2}}\cdot\frac{\sin q\nu\alpha/2}{\sin\nu\alpha/2}\cdot\sin\frac{\nu mq-\varepsilon}{2}\cdot\frac{\sin m\frac{\nu q\alpha-\pi/m}{2}}{\sin\frac{\nu q\alpha-\pi/m}{2}} \quad (5)$$

Equation 5 was used instead of Equation 4 to compute the primary mmf in the Oberretl computer program developed as part of this study.

2.1.3 Primary Harmonic Current Distribution

The Oberretl model substitutes for the actual primary current distribution in the stator, an effective current density (sheet), $\alpha_z(x,z)$, given by

$$\alpha_z(x,z) = \sum_n \sum_\nu J(\nu,n) \cos\frac{n\pi z}{L} e^{j\left(\omega t - \nu x\frac{2\pi}{\ell} + \frac{\pi}{m}\right)} \quad (6)$$

where $J(\nu,n)$ is the amplitude of the Fourier current harmonic for transverse (z-directed) currents, ℓ and L are the length and width repsectively of the "unit periodic cell", and ν and n and the respective harmonic orders along the longitudinal are transverse wave vector directions. The harmonic amplitude, $J(\nu,n)$, is given explicitly by

$$J(\nu,n) = \frac{16\ NI_1\sqrt{2}\ {}^{\nu}k_w\ n_y}{\pi\ell} \quad (7)$$

Here ${}^{\nu}k_w$ is the winding factor for the νth harmonic, $N\ I_1$ the ampere-turns in a single stator slot, and ${}^{n}y$ the amplitude of the transverse dependence of the mmf-distribution.

A. <u>$J(\nu,n)$ dependence on longitudinal harmonic order, ν.</u>

The variation of $J(\nu,n)$ with longitudinal harmonic order is presented in Figure 1 (solid curve) using the motor parameters listed in Section 2.2.1 For the purpose of calculation, the transverse harmonic order, n, was set equal to 1. For the choice of gap length, ℓ_ℓ= 33.212 meters, the peak Fourier harmonic at ν_5 = 198. (197.5) and the effective 7th Fourier harmonic at ν_7 = 277 (276.5). It is interesting to compare the Oberretl harmonic current density function (Equation 7) with the Fourier transform of a single harmonic wave,

$$J(k) = J_1 \frac{\sin\left((k - k_o)\ell_s\right)}{k - k_o} \quad (8)$$

ℓ_s is the distributed length of the current density wave, k the independent wave propagation number equivalent to $\nu mq\alpha/\tau_p$ in the Oberretl model, and k_o the propagation number of the wave equal to π/τ_p. Setting k_o equal to the wave number of maximum $J(\nu,n)$ in Figure 1 and ℓ_s equal to the effective length of the TLRV stator ($\ell_s = P\tau_p$), the dashed curve shown in Figure 1 is obtained

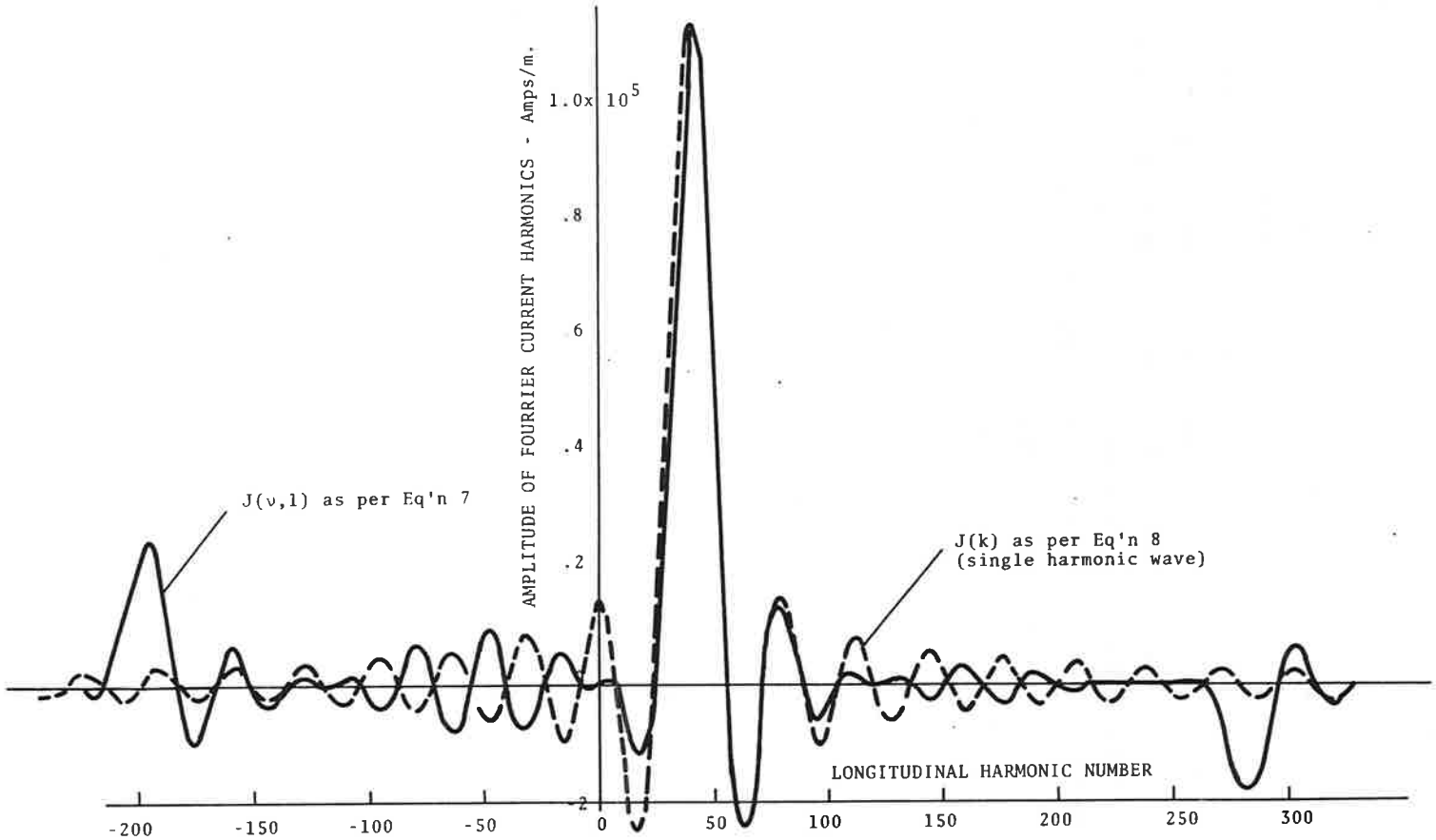

Figure 1. Primary Current Harmonic Amplitude as a Function of Longitudinal Harmonic Number Using TLRV LIM Parameters

for the harmonic current distribution. J_1 in Equation 8 was normalized to the peak amplitude computed from Equation 7. Figure 1 shows that the harmonic spectrum derived from a single-harmonic wave represents a fair approximation to $J(\nu,1)$ in the spectrum region of the principal harmonic contribution, i.e., $10<\nu<70$. Since the contribution of the higher-order harmonics to the LIM reaction forces is comparatively small, the stress tensor components evaluated using the single harmonic transformation (Equation 8) should not be significantly different from those evaluated using the multi-harmonic transform function (Equation 7). Since Yamamura and Oberretl use Equations 8 and 7 respectively to describe the primary harmonic current spectrum, a comparison of the reaction forces computed using the two methods should indicate whether the above conclusion is valid.

B. <u>$J(\nu,n)$ dependence on transverse harmonic order, n.</u>

The Oberretl model assumes the primary current density to vary with transverse displacement as shown in the sketch below. For z-positions within the confines of the primary, i.e., $-c\leq z\leq c$, the primary current density is constant. Beyond the primary edge, the current density decays to zero in a distance h according to $1 - \sin\frac{(z-c)\pi}{2h}$ and remains zero in the regions defined by $c+h\leq|z|\leq L/2$. Oberretl indicates this choice of z-functional dependence for the primary current is somewhat arbitrary and other functional dependences should be used in its place, provided they are consistent with results of field measurements.

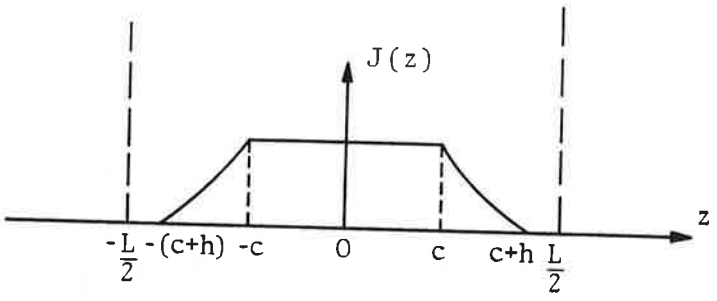

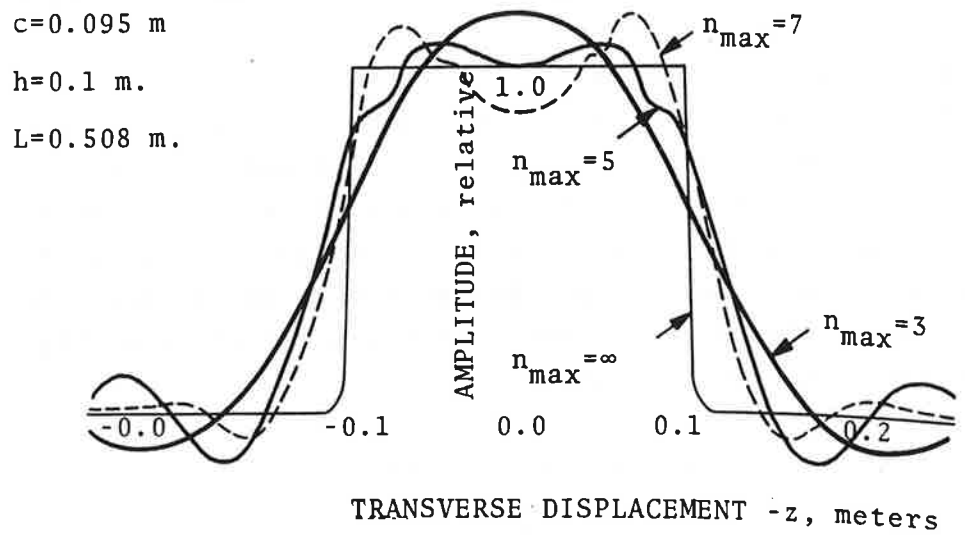

Figure 2. Relative Current Density Amplitude Along Transverse Direction

Oberretl expresses the above current distribution in terms of the Fourier Series

$$\theta(z) = \frac{4}{\pi} \sum_{n} \left\{ \frac{\left(\frac{L}{2h}\right)^2}{\left(\frac{L}{2h}\right)^2 - n^2} \left[\frac{1}{n} \sin \pi n \frac{(c+h)}{L} - \frac{2h}{L} \cos \pi n \frac{c}{L} \right] \right\} \cos n\pi \frac{z}{L} \qquad (9)$$

$n = 1, 3, 5, \ldots$

where the term in brackets {} corresponds to ^{n}y in Equation 7. Figure 2 shows a sketch of $\theta(z)$ as a function of the transverse displacement along the z axis for increasing values of maximum harmonic order, n_{max}, for the TLRV LIM. The larger the value of n_{max}, the better the approximation to the "ideal" current distribution function corresponding to $n_{max}=\infty$. Large n_{max}, however, results in excessive computing time and a compromise is necessary between computational costs and the relative "accuracy" of the current distribution function. In the TLRV and LIMRV LIM calculations described later in the report, n_{max} was chosen equal to the

value used by Oberretl in his LIM calculations, namely, $n_{max}=5$.

The use of a two-dimensional Fourier representation to describe the primary current causes the propagation vector in the secondary along the normal direction to be a function of both longitudinal and transverse wave numbers. This appears to be the basis for the Oberretl claim to a three-dimensional model. It leads to a reduction in the dependence of computed thrust on the longitudinal harmonic number only, which in the case of the Yamamura theory (Ref. 3, p. 98) results in oscillatory-type behavior in the thrust-versus slip characteristics of high speed LIMs near small motor slips.

2.1.4 Thrust Harmonic Amplitude Distribution

The LIM thrust in the Oberretl model is found by summing harmonic thrust contributions over the longitudinal (ν) and transverse (n) harmonic wave orders. If $F(\nu,n)$ is the amplitude of the ν, nth thrust harmonic, the LIM thrust is given by

$$F_x = \sum_{\nu} \sum_{n} F(\nu,n)$$

where

$$F(\nu,n) = \frac{L\ell^2 \lambda \mu_o}{8\pi\nu} J_1^2(\nu,n) \quad \frac{Im(C_{12})}{|\sinh\lambda g + C_{12} \cosh\lambda g|^2} \tag{10a}$$

$$C_{12} = \frac{\sqrt{\lambda^2 + j\omega\mu_2\sigma_2 {}^{\nu}s}}{\lambda\mu_{02}} \tanh\left(\sqrt{\lambda^2 + j\omega\mu_2\sigma_2 {}^{\nu}s} \cdot \frac{b}{2}\right) \tag{10b}$$

λ is the wave number in the airgap along the normal direction, σ_2 is the conductivity in the secondary, μ_2 is the permeability of the secondary equal to $\mu_2=\mu_{o2}\mu_o$, and ${}^{\nu}s$ is the harmonic slip given by ${}^{\nu}s=1-\nu(1-s)mq\alpha/\pi$.

Figure 3 presents a plot of Equation 10 as a function of longitudinal order (ν) for the TLRV LIM at line frequencies of 150, 175, and 200 Hz. For purposes of calculation, the transverse harmonic order was set equal to unity. Motor speed was fixed at 300 mph and line current at 530 amperes corresponding to conditions assumed in the later TLRV LIM calculations. The remaining TLRV parameters used to compute $F(\nu,n)$ are given in Table 1. The figure illustrates several features of the harmonic thrust function.[4] First, $F(\nu,n)$ is large only within a limited range of longitudinal harmonic orders centering on the principal harmonic order ν_o associated with the fundamental wave number. In this example of the TLRV LIM, the principal harmonic order $\nu_o \approx 40$ corresponds to the peak current density as shown in Figure 1. Second, $F(\nu,n)$ is zero at periodic values of longitudinal harmonic order since $J(\nu,n) = 0$ for $\nu = \nu_o(1 \pm 2m/P)$, $(m=1,2,3,..)$. Third, $F(\nu,n)$ shows a rapid change at the singular point $\nu = \nu_o/(1 - \text{slip})$. Special care must be exercised in the numerical integration of $F(\nu,n)$ in the region of the singularity, particularly at frequencies near zero motor slip. Iwamoto[4] suggests the use of finite difference methods for improving the accuracy of the numerical integration in the region of the singularity.

2.1.5 Airgap Flux Density

The LIM flux density distribution in the Oberretl theory is described by an infinite Fourier series of spatial harmonics along the longitudinal and transverse axes of the motor. The components of flux density at the surface of the secondary can be written in the form

$$B_x = \sum_{\nu} \sum_{n} B_o(\nu,n)\, C_{12}\, \cos k_z z\, e^{-j(k_x x - \omega t)} \tag{11}$$

$$B_y = j \sum_{\nu} \sum_{n} \frac{\lambda}{k_x} B_o(\nu,n)\, \cos k_z z\, e^{-j(k_x x - \omega t)} \tag{12}$$

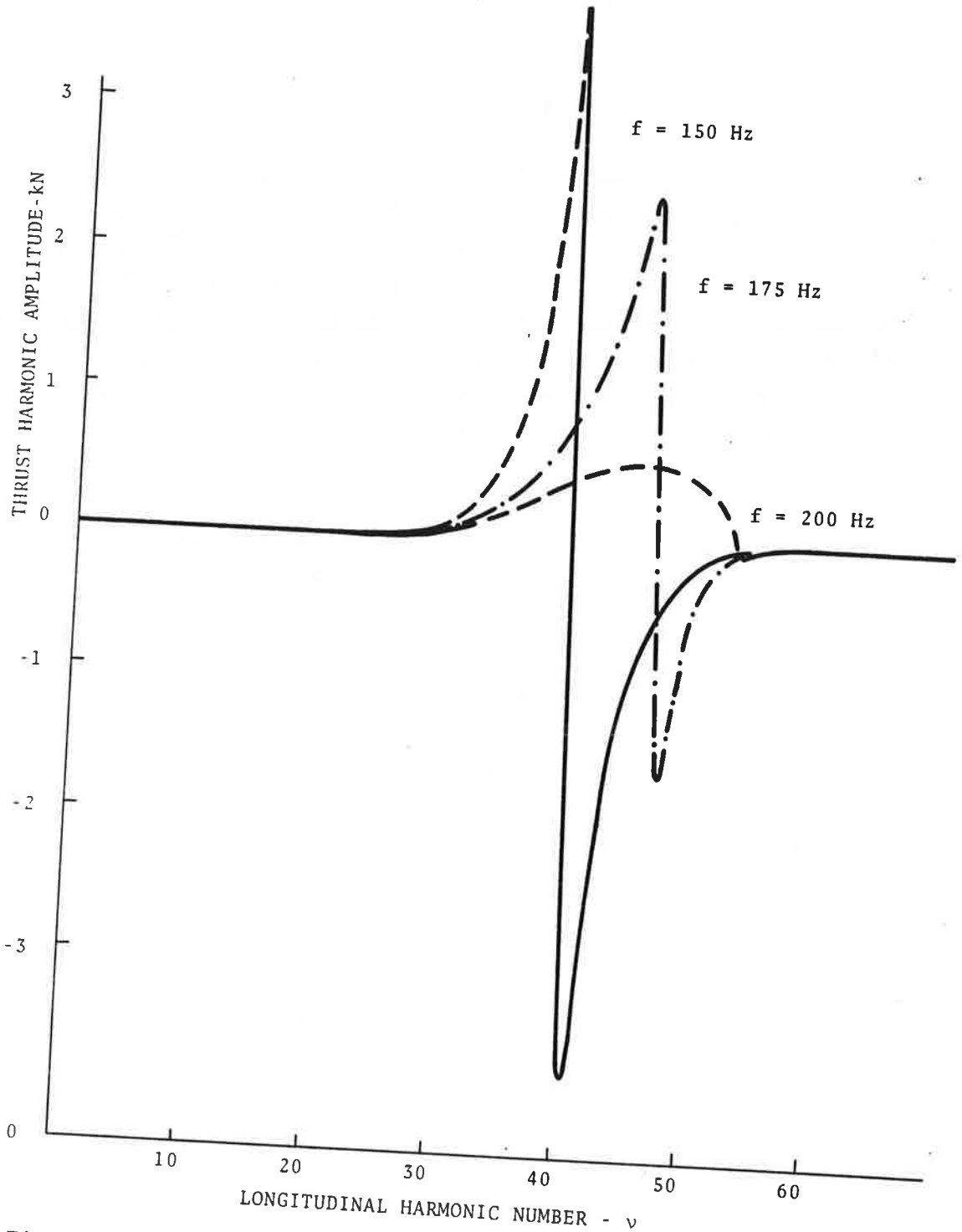

Figure 3. Thrust Harmonic Amplitudes for TLRV LIM at 300 mph. Transverse Wave Number, n=1; I_1=700A

$$B_z = -j \sum_{\nu} \sum_{n} \frac{k_z}{k_x} B_o(\nu,n)\ C_{12}\ \sin k_z z\ e^{-j(k_x x - \omega t)} \qquad (13)$$

where

$$B_o\ (\nu,n) = \mu_o \frac{16N\ I_1 \sqrt{2}\ \nu k_w\ n_y}{\pi \ell_s (\sinh\lambda g + C_{12}\cosh\lambda g)}$$

and K_x, k_z are the wave number components along the x,z axes respectively, i.e., $k_x = \nu 2\pi/\ell$, $k_z = n\pi/L$. C_{12} is defined in Equation 10b.

The flux density components defined by Equations 11 through 13 determine the stress tensor components evaluated at the surface of the secondary. Therefore, the correctness with which these equations describe the flux density in an actual LIM is critical to an accurate calculation of LIM forces. A comparison of the computed flux density components with that obtained from flux mapping in the motor airgap offers a check on the effectiveness of the LIM model to represent an actual LIM.

Figure 4 gives the airgap flux density computed as a function of displacement distance along the transverse axis using parameters appropriate to the TLRV LIM. Motor speed was taken as 300 mph and line frequency as 200 Hz. Three curves are presented corresponding to three different values of maximum transverse harmonic number n_{max}. The curves show that the flux density tends to peak inside the primary region with increasing n_{max}, with the position of maximum flux density occurring near the inside edges of the primary. For $n_{max}=17$, the flux distribution approaches the form predicted by Bolton[5] for DLIMs with symmetric secondaries. The additional peak in flux density which occurs outside the region of the primary is disturbing, since in actual LIMs the flux density tends to decay monotonically with distance from the stator edges. The exact reason for the second peak in the computed flux distribution is not known, but it might be associated with the assumption of a continuous ferromagnetic region in the primary. Its existence raises questions regarding the ability of the

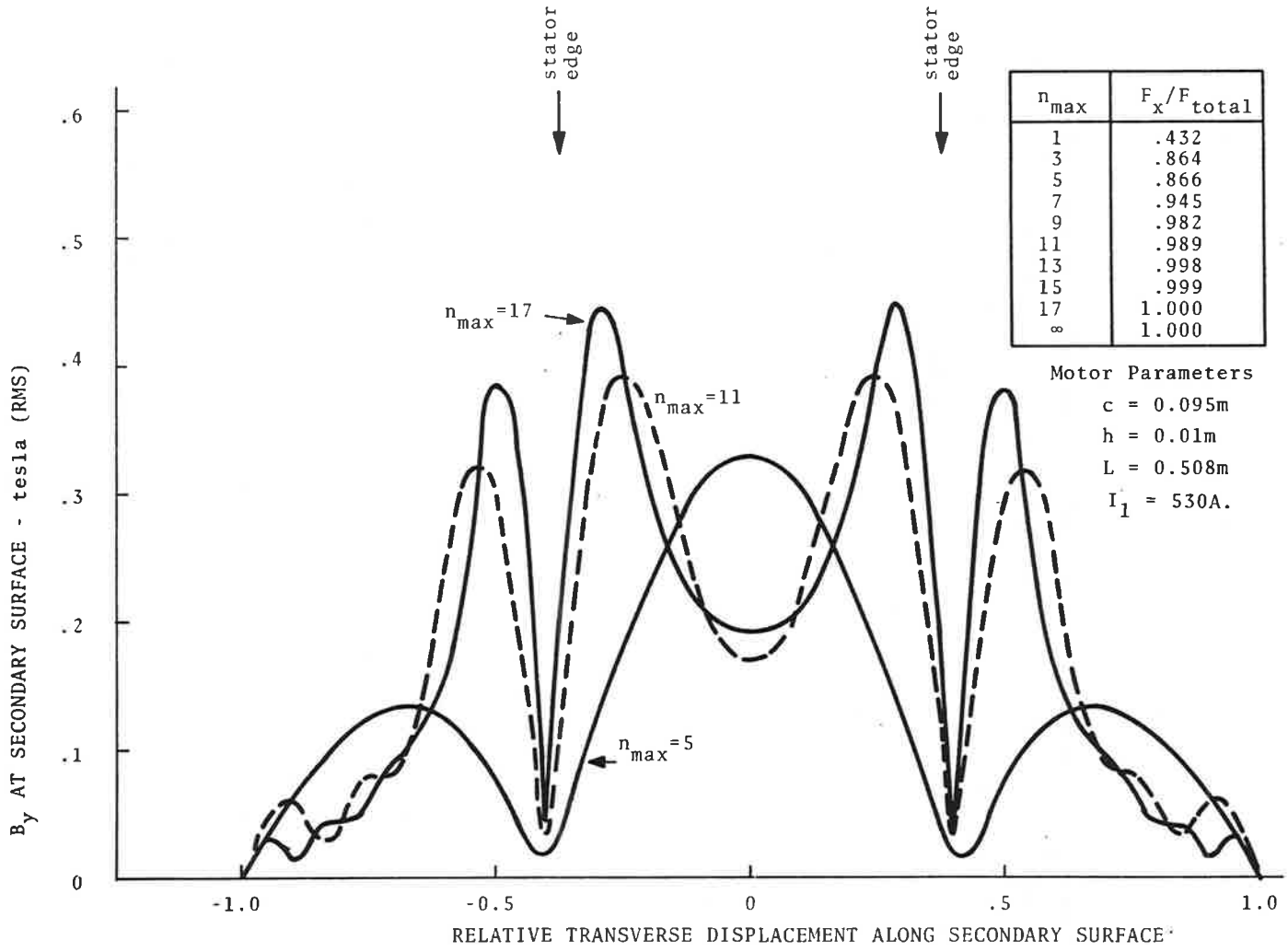

Figure 4. Airgap Flux Density Amplitude Computed for Positions Along Transverse LIM Axis

Oberretl model to describe accurately effects related to the finite width of the motor.

The ratio of thrust for increasing n_{max} values normalized to the thrust for n_{max}=25 is shown in tabular form in Figure 4. The table shows an increase in computed thrust with increase in n_{max} for this LIM example; at n_{max}=7, the thrust is 95 percent of the value computed for n_{max}=25. In view of the irregular behavior of the flux density distribution along the transverse axis and dependence on n_{max}, it is not clear whether the thrust is computed with greater accuracy when n_{max} is larger as compared with n_{max} of a smaller specified value. The additional peak in flux density which occurs outside the region of the primary is disturbing, since in actual LIMs the flux density tends to decay monotonically with distance from the stator edges. The origin of the second peak might be associated with the Oberretl assumption of a continuous ferromagnetic primary, which tends to enhance the flux density in the regions outside the stator edges. It is of some interest that the phase computed for the second peak is approximately 180 degrees different from that computed for the first peak, a result which is consistent with the relative phases anticipated for flux produced by secondary edge currents in the absence of magnetic edge effects. The large discrepancy between computed and actual flux densities in the regions outside the primary raises questions regarding the effectiveness of the Oberretl model to predict effects arising from the finite LIM width.

2.2 COMPUTER STUDY OF TLRV AND LIMRV LIMs USING OBERRETL MODEL

The following sections summarize results of computer studies of TLRV and LIMRV motors, using a computer program based on the Oberretl model. All computations were performed using the PDP-10 Computer located at the Transportation Systems Center, Cambridge, Massachusetts. Computer times required for typical runs comprising ten cases (variable slip or frequency) were of the order of 60 seconds.

2.2.1 TLRV Linear Induction Motor

The TLRV thrust and normal forces were computed for a fixed input line current of 700 amperes and motor speed of 300 mph (134.1 m/s). The motor parameters used in the calculations are given below. The dimensions of the motor 'unit cell' forming the basis for the two-dimensional periodic array are shown in Figure 5. The longitudinal and transverse mmf gap lengths were taken respectively at 33.212 and 0.199 meters. Longitudinal (ν) harmonics were summed over the range $-120 \leq \nu \leq 120$. Transverse (n) harmonics were summed from n = 1, 5, i.e., n = 1, 3, and 5.

TLRV Motor Parameters

Turns per Coil (N) = 4
Pole Pitch (τ_p) = .448 m.
Core Width (2c) = .1905 m.
Poles (P) = 5
Core Length (ℓ_s) = 2.56 m.
Air Gap (g) = .0171 m.
Phases (m) = 3
Slots per Phase (q) = 5
End Half-filled Slots (ε) = 5
Secondary Thickness (b) = .0066 m.
Secondary Resistivity (ρ) = $.416 \times 10^{-7}$ ohm-m.
Coil Overhang (h) = .01 m.
Longitudinal MMF Gap (ℓ_s) = 33.212 m.
Transverse MMF Gap = .199 m.

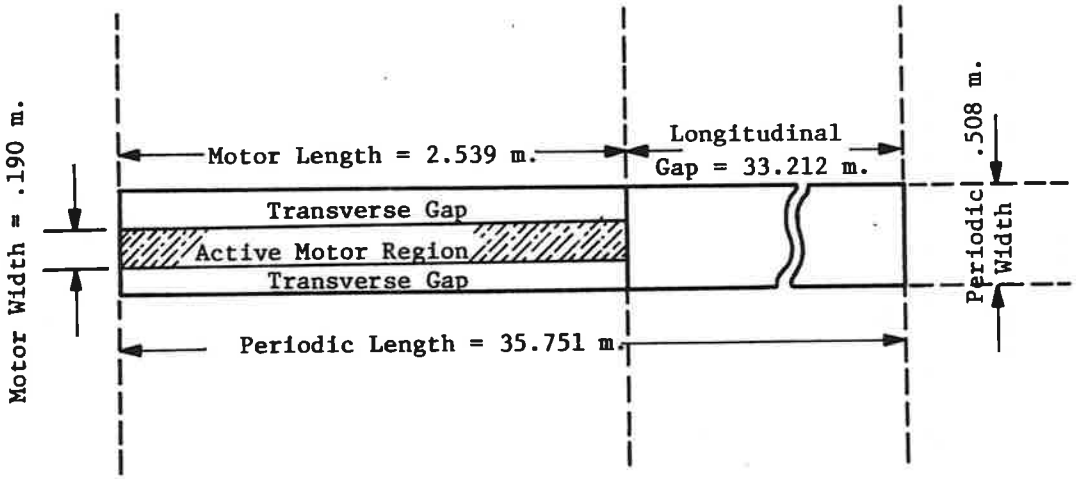

Figure 5. MMF Unit Cell Used in TLRV LIM Calculations

Longitudinal Periodic Wavelength = 35.772 m.
Transverse Peiodic Half-wavelength (L) = 54 m.
Motor Speed (V) = 134.1 m/s

2.2.2 TLRV Thrust-Frequency Characteristics

The TLRV thrust computed for frequencies in the range of 155 to 200 Hz is shown in Figure 6. The corresponding thrust predicted by Elliott[2] is also presented for comparison. The thrusts computed using the Oberretl model are about one-third larger than those computed by Elliott. The choice of longitudinal mmf gap length was sufficiently long to insure effective damping of the end-effect wave inside the periodic length defined by the "unit cell" of the motor.

It is interesting to speculate on the reasons for the divergent thrust predictions. The computer analysis of Elliott includes current and magnetic end-effects and assumes finite lengths for both the mmf and primary ferromagnetic regions. In contrast, the Oberretl analysis neglects ferromagnetic end-effects; however, as Yamamura (Ref. 2, p. 67) points out, this should have a relatively small effect on the value of computed thrust. In the Fourier series representation of primary mmf, only three harmonic terms were included in the summation of transverse wave numbers, i.e., n = 1, 3, 5, in the Oberretl computer program. If additional harmonic terms had been included in the summation, it is likely that the thrust predicted by Oberretl would increase slightly since thrust is directly proportional to $(^{n}y)^{2}$ or the square of the transverse harmonic amplitude defined by Equation 2. This, however, would cause the Orberretl-Elliott thrust predictions to diverge even more than indicated in Figure 6.

2.2.3 TLRV Normal Force-Frequency Characteristic

The corresponding normal forces computed as a function of frequency are shown in Figure 7 for the TLRV. Elliott's results computed for the same conditions are indicated by the dashed curve. Both results predict a zero force crossover frequency near 190 Hz. Oberretl's theory gives considerably larger normal forces

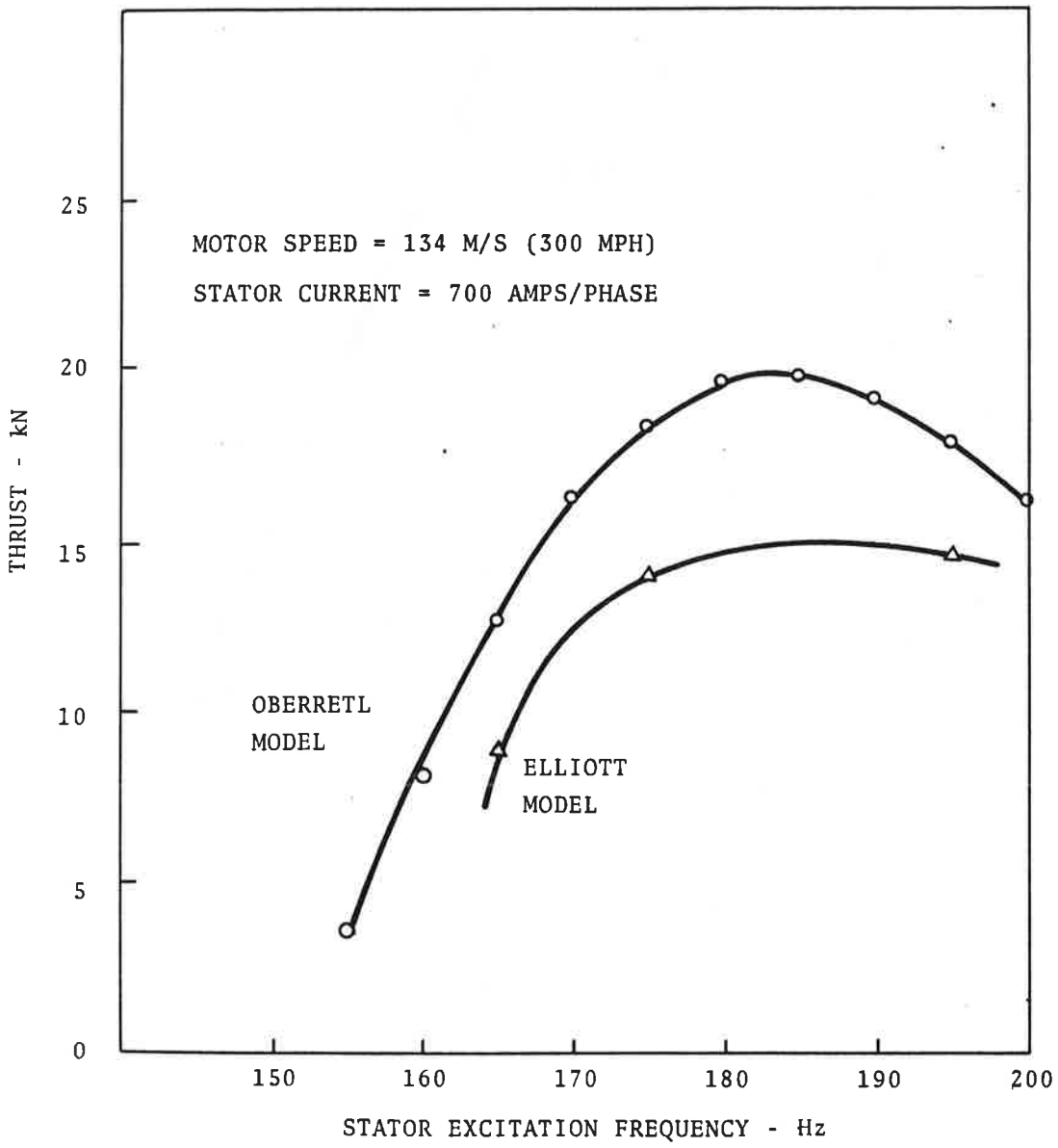

Figure 6. Computed TLRV LIM Thrust as a Function of Driving Frequency

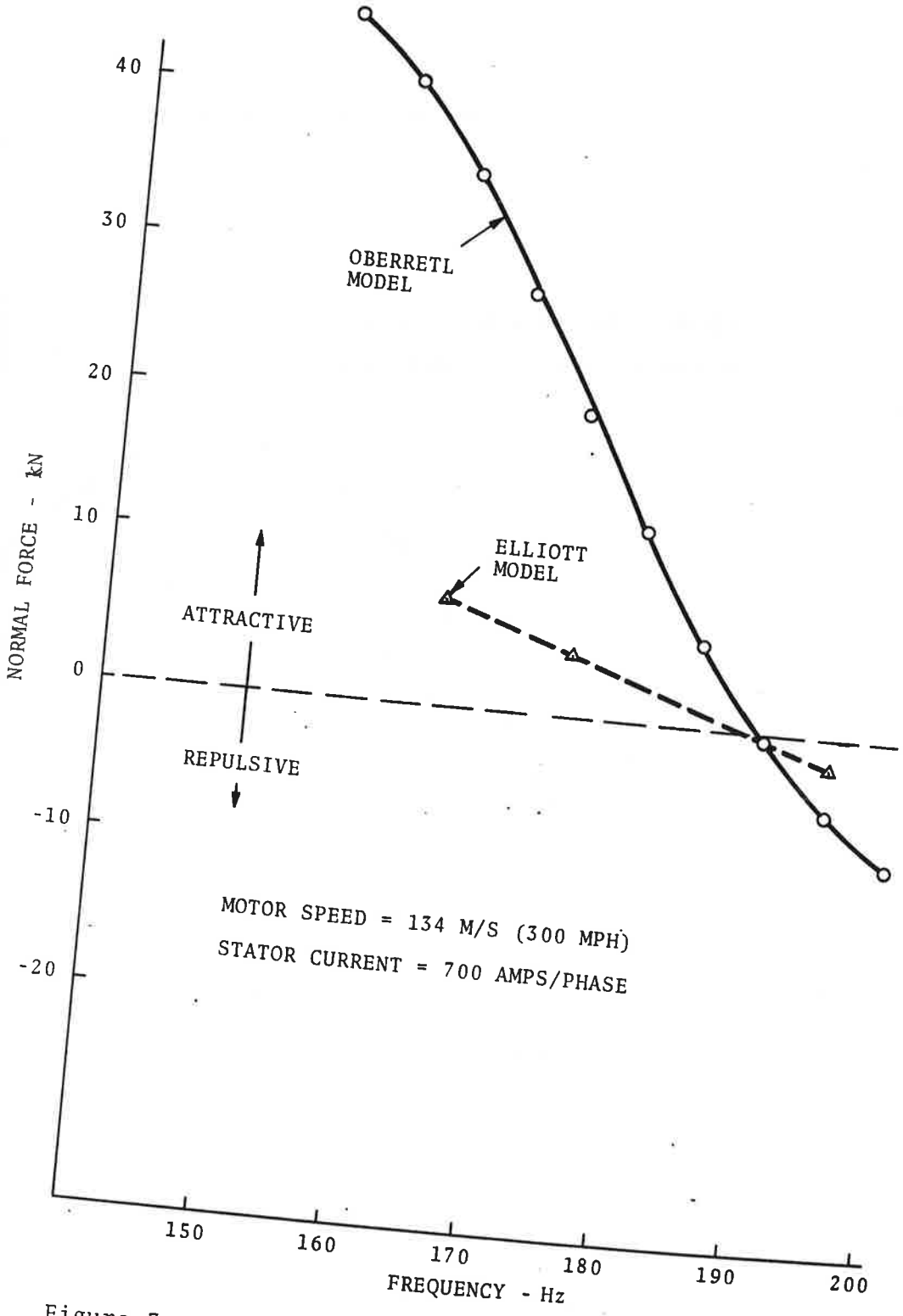

Figure 7. Computed TLRV LIM Normal Force as a Function of Frequency

than does Elliott's at frequencies below the crossover point. Such a large discrepancy in predicted forces is believed associated with the failure of the Oberretl theory ("infinite iron") to include the effect of finite primary ferromagnetic region in the LIM model. This causes the Oberretl theory to overestimate the normal attractive force component as a result of overestimating the trailing end-effect wave and edge-effect flux along the sides of the motor.

It is helpful in understanding the origin of the large normal forces to attempt a rough calculation of the attractive component of normal force at zero slip where it is maximum and the predominant component of normal force. The magnetic force can be expressed in terms of the normal component of flux density, B_y (Ref. 6, p.55)

$$F_n = \frac{1}{2\mu_o} (B_y)^2_{ave} \text{ Newtons/meter}^2 \qquad (14)$$

The airgap flux density is given approximately by

$$B_y = \frac{\mu_o N I_1 \sqrt{2}}{g} q \cdot \frac{3}{2} 1.11 \, e^{j(\omega t - kx)} \qquad (15)$$

If one assumes the airgap flux density to be reduced by the end-effect by a factor of two when averaged over the length of the motor, then Equation 14 gives for the normal attractive force,

$$F_n = 11.7 \text{ kN (attractive)} \qquad (16)$$

This compares closely with the value of attractive normal force computed by Elliott for a frequency of 165 Hz equal to 9.35 kilonewtons. The Oberretl theory yields a considerably larger value of normal (predominantly attractive) force near zero slip equal to approximately 26 kilonewtons, or 2-1/2 times that of Elliott. This latter is explicable if one assumes the end-effect wave in the mmf gap region contributes a normal force component equal to that contributed by the active motor region.

2.2.4 LIMRV Linear Induction Motor

The LIMRV thrust and normal forces were computed for a fixed input line current of 2400 amps and motor speed of 250 mph (112 m/s). The relevant motor parameters used in the calculations are listed below. The dimensions defining the motor 'unit cell' are given in Figure 8. The longitudinal and transverse mmf gap lengths were chosen respectively equal to 11.096 and 0.150 meters. The longitudinal gap length was equal to about 1-1/2 times the estimated decay length at 165 Hz computed using Equation 1. Longitudinal harmonics were summed over the range $-50 \leq \nu \leq 50$. Transverse harmonics were summed from n = 1, 5, or n = 1, 3, and 5. The choice of maximum longitudinal harmonic number of 50 was adequate to include the significant components of Fourier current harmonic since the main current harmonics centered closely about $\nu = 21$ (20.9).

LIMRV MOTOR PARAMETERS

Turns per Coil (N) = 1
Pole Pitch (τ_p) = .355 m.
Core Width (2c) = .254 m.
Poles (P) = 10
Core Length (ℓ_s) = 3.81 m.
Air Gap (g) = .024 m.
Phases (m) = 3
Slots per Phase (q) = 5
End Half-filled Slots (ε) = 5
Secondary Thickness (b) = .0071 m.
Secondary Resistivity (ρ) = 0.416×10^{-7} ohm-m.
Coil Overhang (h) = .01
Longitudinal MMF Gap (ℓ_ℓ) = 11.096 m.
Transverse MMF Gap = .150 m.
Longitudinal Periodic Wavelength = 14.906 m.
Transverse Periodic Half-wavelength (L) = .534 m.
Motor Speed (V) = 112 m/s

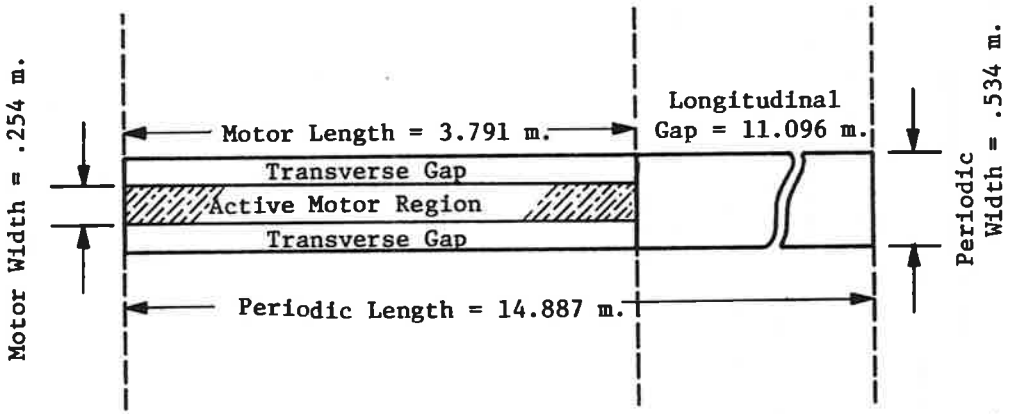

Figure 8. MMF Unit Cell Used in LIMRV LIM Calculations

2.2.5 LIMRV Thrust-Frequency Characteristic

The LIMRV thrust characteristics were computed for pole gap separations of 38.1 mm and 47.6 mm for frequencies ranging from 160 to 200 Hz. Figure 9 summarizes the results of the calculations given by the solid curves. The dashed curve presents the corresponding thrust prediction by Elliott for the case of the 47.6 mm pole gap separation. A single point indicating the thrust predicted by Elliott for a pole gap separation of 38.1 mm and frequency of 175 Hz is also shown.

The agreement of the computed thrusts predicted by the Oberretl and Elliott models is good for the case of pole gap separation equal to 47.6 mm. When compared with the corresponding results for the TLRV thrust (Figure 6), the predicted thrusts are in considerable better agreement for the LIMRV than for the TLRV motor. This can probably be attributed to the larger number of poles and lower operating speed of the LIMRV compared with the TLRV; i.e., end-effects in the LIMRV are less pronounced than in the TLRV.

The change of thrust with pole gap separation is governed by two factors. If end-effects can be neglected (which they cannot in the present case), then the thrust must increase with reduced gap separation, since the airgap flux density must increase with smaller gap separations while holding primary current fixed. The situation is more complicated with end-effect present, however, since reducing the gap separation tends to enhance the end-effect wave. Note that the attenuation constant of the end-effect wave decreases with reduced gap separations. (Ref. 3, p. 26.) The relative importance of these factors will determine the direction in which the thrust will vary with change in pole gap separation. For the thrust to decrease with decrease in gap separation, as predicted by Elliott, the end-effect wave must dominate the driven wave in the airgap region of the motor.

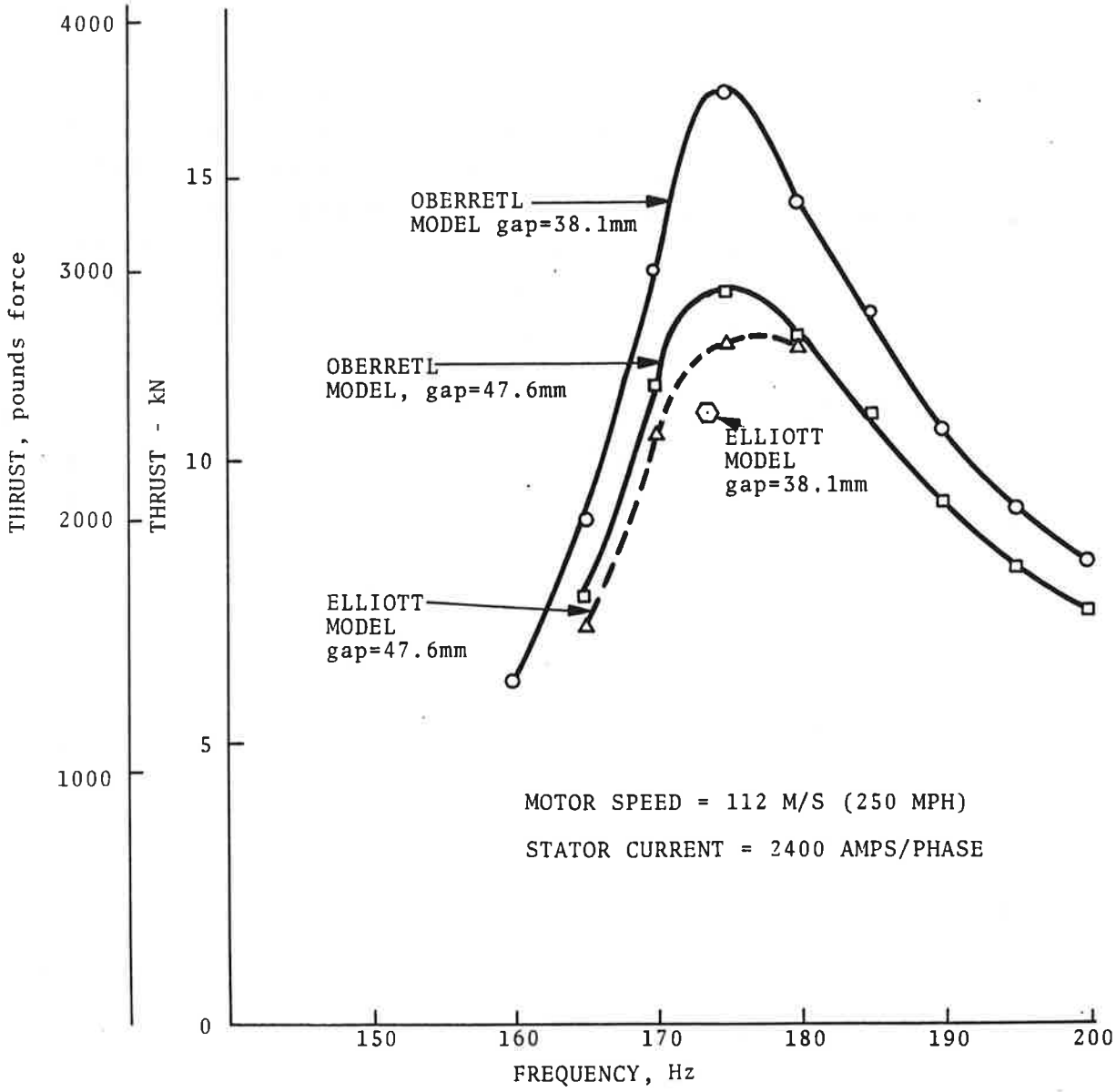

Figure 9. Computed LIMRV Thrust as a Function of Driving Frequency

2.2.6 LIMRV Normal Force-Frequency Characteristic

The corresponding normal forces computed for the LIMRV are shown in Figure 10 for the Oberretl model (solid curces) and the Elliott model (dashed curve). As for the case of the normal forces computed for the TLRV linear induction motor, the Oberretl theory yields force values at low slips equal to about twice those predicted by Elliott. The conclusions derived from the study of the TLRV force characteristics apply here as well; namely, the Oberretl theory over-estimates the normal forces at low slip frequencies (below the zero force crossover frequency) due to its neglect of magnetic end-effects.

A calculation of the attractive component of normal force, similar to that undertaken for the TLRV, is also appropriate here in order to estimate its magnitude near zero slip. Using Equation 14 and assuming a line current of 2400 amps, pole gap separation distance of 47.6 mm, the estimated attractive component of normal force at zero slip is 6.2 kilonewtons. This compares closely with the value of attractive force (component) computed by Elliott equal to 6.2 kilonewtons at 165 Hz.

2.2.7 LIMRV SLIM

The forces which the LIMRV develops when operated in a single-sided mode will now be examined. The secondary will be assumed to have iron backing of infinite permeability, with the backing continuous over the complete back surface of the secondary. The solution of the magnetic diffusion equation for this SLIM model then becomes identical to the DLIM if in the diffusion equations, the thickness of the secondary is replaced by twice the actual thickness of the secondary. This becomes apparent if one considers the boundary conditions at the mid-plane of the DLIM and the corresponding boundary conditions at the secondary-iron backing interface of the SLIM.

Wang (Ref. 6, p. 53) has derived expressions for SLIM reaction forces with back iron present. The form of his solutions suggests that SLIM thrust varies inversely with secondary thickness when

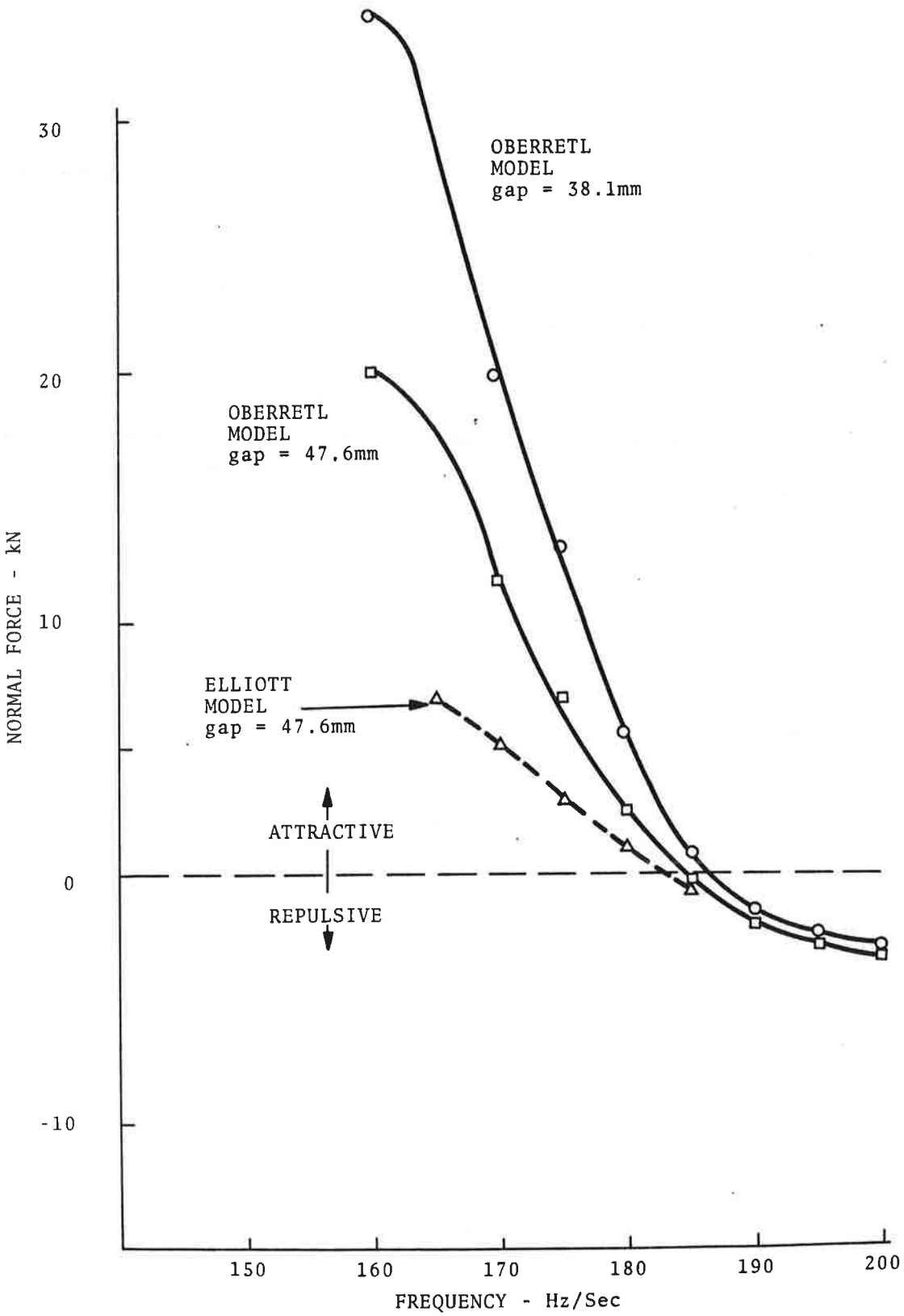

Figure 10. Computed LIMRV Normal Force as a Function of Driving Frequency

the thickness is small compared with the wave propagation number in the secondary. Since the latter condition is compatible with the assumptions made in the Oberretl analysis, one would anticipate the same functional dependence on secondary thickness to result with the Oberretl program.

2.2.8 LIMRV SLIM Thrust-Frequency Characteristic

The computed SLIM thrust for the LIMRV operating with a phase current of 1200 amps and motor speed of 250 mph (112 m/a) is shown in Figure 11. The airgap distance was chosen nominally at 24 mm. The peak thrust of 4300 newtons, or approximately 1 kilopound, occurs near 175 Hz. The reduction in thrust of the single-sided motor as compared with the double-sided version can be seen by referring to Figure 10 for the case of the 47.6 mm gap. One can conclude that in order to develop SLIM thrusts comparable to DLIM thrusts, it will be necessary to reduce the thickness of the secondary element. This assumes, of course, that all other conditions remain fixed in the process.

2.2.9 LIMRV SLIM Normal Force-Frequency Characteristic

The corresponding normal forces computed for the LIMRV in the SLIM mode are shown in Figure 12. The curve indicates that the zero-force-crossover-frequency is lowered when the LIMRV is operated in the SLIM mode as compared with the DLIM mode. The conclusions appropriate to the previous calculations of LIM normal forces also apply here.

2.3 THRUST DEPENDENCE ON SECONDARY THICKNESS AND ELECTRICAL CONDUCTIVITY

Oberretl expresses the total LIM thrust as the summation of harmonic thrusts, defined by Equation 10, over the respective longitudinal and transverse wave numbers characterizing the two-dimensional array. The dependence of thrust of secondary thickness, b, and electrical conductivity, σ_2, is contained in the C_{12} term which enters in both numerator and denominator of the thrust harmonic expression. In the thin-sheet approximation in which

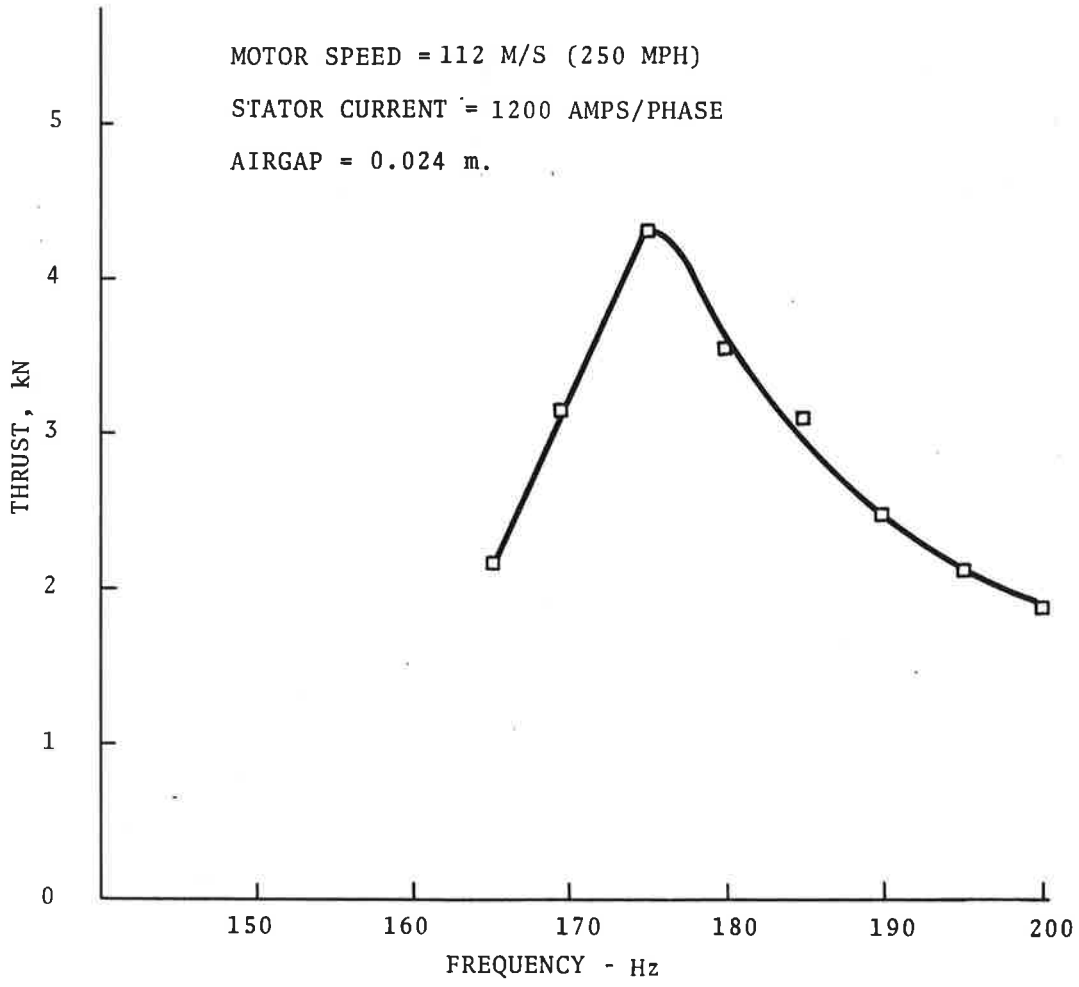

Figure 11. Computed LIMRV-SLIM Thrust as Function of Driving Frequency

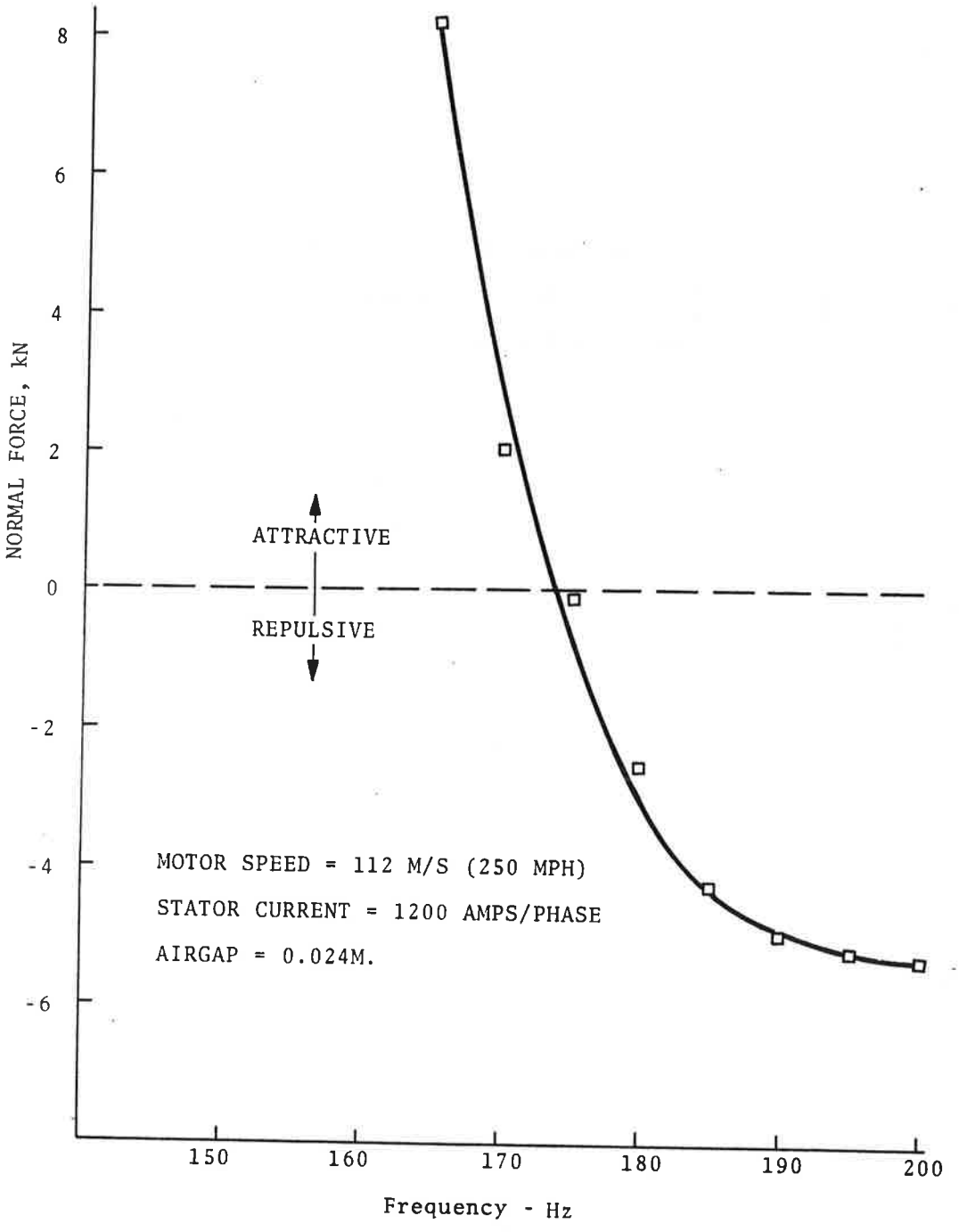

Figure 12. Computed LIMRV-SLIM Normal Force as Function of Driving Frequency

$\left| \sqrt{\left(\frac{\nu 2\pi}{\ell}\right)^2 + \left(\frac{n\pi}{L}\right)^2 + j\mu_2 \omega \sigma_2 {}^{\nu}s} \right| \cdot \frac{b}{2} << 1$, the thrust can be rewritten as

$$F_x \approx \frac{L\ell^2}{16\pi} \sum_n \sum_\nu \frac{\mu_o^2}{\nu} J_1^2(\nu,n) \left\{ \frac{\omega^{\nu} s \sigma b}{\left(\sinh\lambda g + \frac{\lambda b}{2}\cosh\lambda g\right)^2 + \left(\frac{\omega^{\nu} s \mu_2 \sigma_2 b}{2\lambda}\cosh\lambda g\right)^2} \right\} \qquad (17)$$

2.3.1 LIM Thrust-Versus-Secondary Thickness

Consider the example of the TLRV linear induction motor. The thrust computed according to the Oberretl theory, using Equation 13, is given in Figure 6. For the motor speed of 300 mph, maximum thrust occurs at 185 Hz or a slip frequency of 35 Hz. The substitution of this value of slip frequency in Equation 13 shows that the frequency-dependent term in the denominator of the bracket dominates the frequency-independent term for wave harmonics lying in the region of the fundamental wave harmonic. In this case, Equation 13 predicts that thrust will increase inversely with secondary thickness.

The peak thrust must ultimately decrease (to zero) as the secondary thickness approaches zero, so that maximum thrust must obtain for a certain value of b. The critical thickness for maximum peak thrust is given by

$$b = \frac{2\lambda \tanh\lambda g}{\mu_o {}^{\nu} s \omega \sigma_2}$$

For a typical high-speed LIM with nominal secondary thickness value, the thrust in the region of maximum thrust can be expected to increase with a decrease in secondary thickness. Whether this increase in thrust can be realized in practice depends on practical considerations involving power dissipation and structural strength of the secondary element. Laboratory tests on the effect

of secondary thickness would provide the most direct means for verifying the above predictions and checking the validity of the theory as applied above.

2.3.2 LIM Thrust-Versus-Secondary Electrical Conductivity

The dependence of LIM thrust on secondary electrical conductivity is contained in the bracket term in Equation 17. For a high-speed linear induction motor operating near peak thrust, the conductivity-dependent-term in the denominator dominates the remaining terms. Theory predicts, therefore, that the peak thrust should increase with decrease in secondary electrical conductivity, until the condition is reached whereby the conductivity-dependent-term in the denominator has a magnitude equal to that of the remaining term in the denominator. Further decreases in conductivity should reduce the peak thrust of the LIM.

As in the previous discussion of the effect of secondary thickness on LIM thrust, laboratory studies would be helpful in verifying trends predicted by the Oberretl theory as it relates to thrust dependence on secondary conductivity.

3. CONCLUSIONS

A computer program was written to calculate the thrust and normal forces in a constant current-driven linear induction motor using the theoretical treatment of Oberretl. The program was applied to evaluate the forces in the TLRV & LIMRV motors and the results compared with similar calculations performed by D. Elliott (JPL) using a different computer program model.

The Oberretl computer program gave thrust values which were in good agreement with Elliott's values for the LIMRV motor but about 20 percent greater than Elliott's predictions for the TLRV. The variation in computed thrust characteristics given by the different programs is partly related to end-effects and the manner in which they are taken into account in the numerical analyses. Since the TLRV operates at higher speeds, has fewer pole numbers, and smaller length, end-effects would be expected to have more effect than with the LIMRV.

The normal forces computed with the Oberretl program were consistently greater than Elliott's predicted forces at frequencies below the zero-force-crossover frequency. Estimates of the normal force at zero slip proved more consistent with Elliott's predictions than with Oberretl's. Since the Elliott computer program used a LIM model having a finite primary ferromagnetic length and width, his program would be expected to yield more accurate reaction force predictions than those obtained using the Oberretl program. This would apply particularly to the calculation of normal forces in which the Oberretl assumption of continuous primary ferromagnetic region leads to excessively large (attractive) normal forces near zero slip.

The Oberretl analysis makes no allowance for the finite length of the primary ferromagnetic region. It therefore neglects magnetic end-effects and treats only end-effects related to a finite primary current distribution. A similar approach is undertaken by Yamamura[3] using a Fourier transform method instead of the Fourier Series representation of Oberretl. Yamamura sums the

stress tensor (or JxB) component, evaluated at the primary surface, over the length of the primary while Oberretl sums the stress tensor components, evaluated at the secondary surface, over the length of the motor unit cell. Both methods should, in principle, give equivalent results. In considering the effect of finite LIM width, Yamamura uses the results of Bolton's treatment of edge-effects[5] to correct his answer for finite width of the primary current excitation. The Oberretl approach is different in that edge-effects are brought into the treatment in the same manner as are end-effects: namely, by describing the current and field spatial distributions in terms of a series of two-dimensional spatial harmonics. It is seen that the Oberretl method leads to unreasonable predictions for the flux densities in the regions outside of the edges of the motor for the LIM example examined in this report. The Oberretl treatment of edge-effects bears closer scrutiny in order to assess its implications in the evaluation of LIM reaction forces.

The Oberretl treatment is limited to LIMs with even numbers of poles. This limitation can be traced to the winding distribution factor, which has been derived for even pole numbers. An alternate expression for the winding factor is given in this report, which is believed to correctly describe the mmf distribution of primaries comprising both even and odd numbers of poles.

REFERENCES

1. Oberretl, K., "Three-Deminsional Analysis of the Linear Motor Taking into Account Edge-Effects and the Distribution of the Winding," Archiv fuer Electrotechnik, 55, No. 4, 1973.

2. Elliott, D., Communication to M. Guarino, March 29, 1974.

3. Yamamura, S., Theory of Linear Induction Motors, John Wiley & Sons, New York, NY, 1972.

4. Iwamoto, M., Ohno, O., Itoh, T., and Shinryo, Y., "End-Effect of High Speed Linear Induction Motor." IEEE Transactions on Industry Applications, Vol IA-9, No. 6, Nov./Dec. 1973.

5. Bolton, H., "Transverse Edge-Effect in Sheet-Rotor Induction Motors," Proc. IEE, Vol. 116, No. 5, May 1969.

6. Wang, T.C. and Lipkis, R.S., "Single-Sided Linear Induction Motor (SLIM), A Study of Thrust and Lateral Forces," TRW Systems Group, Report FRA-72-25, June 1971.